


# Conceptual model to quantify uncertainty in steady-RANS dissipation closure for turbulence behind bluff bodies

Zengrong Hao \* and Catherine Gorlé

*Wind Engineering Laboratory Department of Civil and Environmental Engineering, Stanford University, Stanford, California 94305, USA*



(Received 18 March 2021; accepted 1 November 2021; published 21 January 2022)

In turbulent bluff body flows, the presence of vortex shedding, a form of coherent structures (CS), introduces a new characteristic scale that is distinct from the scale of background stochastic turbulence (ST). This double-scale picture essentially invalidates the conventional single-scale modeling for the turbulence energy dissipation in steady Reynolds-averaged-Navier-Stokes (RANS) simulations. In this paper, we present a conceptual model to quantify the uncertainty in the steady-RANS dissipation closure for flows past bluff bodies with vortex shedding. This model is developed in two steps. First, we formulate a double-scale, double-linear-eddy-viscosity (DSDL) framework for the transport of CS and ST energy, with an undetermined energy transfer rate from CS to ST. In this framework, the dissipation of ST energy follows a conventional transport model; the length scale of CS is determined such that the CS energy is intensely produced in free shear layers. Second, we design a functional form for the energy transfer rate based on a qualitative analysis and an analogy with the “return-to-isotropy” process. This form contains two uncertain parameters that control the CS-ST interaction. Subsequently, the DSDL model is tested on simulations of the flows past circular and square cylinders, and of the flow in a pin-fin array. In all cases, the model provides a significant improvement upon both conventional models and models with Reynolds stress shape perturbations. The sizes of the recirculation zones are accurately predicted, and simulations with varying values for the uncertain parameters predict intervals for the peak turbulence kinetic energy that encompass reference data.

DOI: [10.1103/PhysRevFluids.7.014607](https://doi.org/10.1103/PhysRevFluids.7.014607)

## I. INTRODUCTION

Reynolds-averaged-Navier-Stokes (RANS) modeling remains a popular approach for numerical simulations of turbulent flows aimed at engineering analysis and design. Their low computational cost is especially beneficial when a large number of simulations is required, such as for optimization and uncertainty quantification. Despite the frequent use of RANS in engineering analysis, the inaccuracies introduced by the turbulence models that close the RANS equations pose a challenge when the results are used to inform design decisions. Uncertainty quantification (UQ) of the turbulence models, aimed at providing predictions with confidence intervals, could address this challenge.

UQ methods for turbulence models generally consider the relaxation of one or more model assumptions. Specifically for steady-state, single-point RANS closure models based on the linear-eddy-viscosity (LEV) hypothesis, UQ studies have considered the relaxation of free coefficients [1–5], shear stress or eddy-viscosity values [6,7], empirical functional forms in the model equations

---

\*haozr16@stanford.edu

[8–10], and the LEV assumption itself [11–15]. The latter approach, which directly perturbs the shape and/or orientation of the Reynolds stress (RS) tensor, allows departure from the original model form, thus providing a more general framework that has been applied with a variety of perturbation strategies [16–20].

Gorlé *et al.* [12] and Iaccarino *et al.* [14] analyzed the reasoning behind the RS shape and/or orientation perturbation approach. They indicated that the approach’s bounding behaviors for quantities of interest (QoIs) are, to a large extent, attributed to its bounding behaviors for the production term  $\mathcal{P}$  in the transport equation of turbulence kinetic energy  $k$ ; thereby a perturbation to the RS shape and/or orientation indirectly alters  $k$ , a pivotal variable that directly influences the general level of mean momentum transport. This mechanism of perturbation propagation has practically functioned well in terms of bounding the QoIs in the above relevant references. However, failures have been observed near the large separation regions in some cases, where  $k$  was significantly underestimated (by up to 90%) consistently by all the simulations with various  $\mathcal{P}$ -increasing perturbations [21,22]. Some other studies without model perturbations also found such type of severe underestimations [23,24], which are plausibly improbable to be effectively corrected by only perturbing the RS shape and/or orientation. Formally, these observations imply that this failure mode of RANS models is unlikely to originate in the LEV assumption that controls the RS shape and orientation, but instead originates in the closure for the turbulence energy dissipation rate  $\varepsilon$ .

In flow physics, the severe underestimation of  $k$  near large separation regions is closely related to the presence of vortex shedding [25–28], which is a typical form of large-scale coherent structures (CS) associated with the free shear layer instability (see Bonnet and Delville [29] for a general review). Different from the chaotic nature of standard turbulence [termed “stochastic turbulence” (ST) in this work], CS exhibit semideterministic and quasiperiodic dynamics, and are embedded inside and interact with the background ST. A natural approach for handling such a CS-ST system within the RANS framework is to assume some degree of timescale separation between CS and ST and use unsteady simulations to partially resolve the CS. A variety of methodologies to adjust original steady-RANS models to unsteady-RANS has been proposed (e.g., [30–34]). Nevertheless, the substantially larger computational cost of unsteady simulations is a limiting factor in large-scale engineering applications. These facts together raise the question of whether the CS effects can be evaluated more efficiently within the steady-RANS framework that formally averages out both types of fluctuations.

For steady-RANS modeling, the presence of CS causes a fundamental problem for the  $\varepsilon$  closure: without distinguishing CS from ST, one has to assume that both types of fluctuations have identical characteristic velocity and length scales, and thus identical dissipation behaviors. Obviously, this is an oversimplification. ST with a high enough Reynolds number generally has a smooth and partially scale-invariant energy spectrum; in contrast, the spectrum of CS is characterized by local “peaks” [35] without an apparent energy cascade towards a considerably smaller scale [Fig. 1(a)]. When CS are embedded inside ST, the former can lose their energy to the latter by breaking into smaller turbulent eddies via a series of mechanisms (see [36–39] for the CS evolution in free shear layers), which differ in nature from the turbulence cascade in the inertial range. This “double-scale” picture, which was first postulated by Townsend [40], is beyond the capability of conventional RANS models that use a single scale to characterize all the fluctuations and indiscriminately formulate their dissipation; instead, a mechanism to evaluate the effects of CS on the dissipation closure should be incorporated for steady-RANS modeling.

The objective of this paper is to present a conceptual model for quantifying the uncertainty in steady-RANS dissipation closure for turbulent flows with coherent structures. We focus on CS of the vortex shedding type in bluff body flows and develop the model in two steps:

(1) We formulate a double-scale, double-LEV (DSDL) framework for the transport of CS and ST energy separately, with an undetermined energy transfer rate from CS to ST. In this framework, the dissipation of ST energy is assumed to follow a conventional transport model; the length scale of CS is algebraically associated with the mean flow field, such that CS energy is intensely produced in free shear layers.

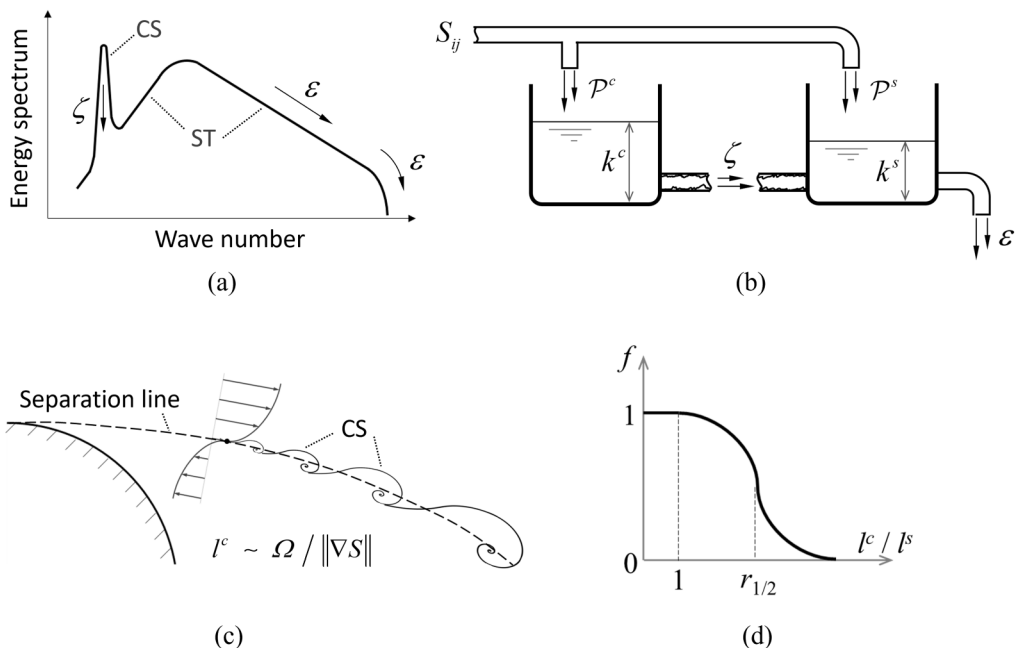


FIG. 1. Principle of the DSDL model: (a) Sketch of a turbulent energy spectrum with coherent structures; (b) tank-tube system analogy for the spectral energy transfer; (c) the supposition of the CS length scale, which naturally yields intense generation of  $k^c$  near the separation line behind a structure; and (d) the assumed function to represent the effect of length scale separation on the CS-ST energy transfer.

(2) We design a functional form for the energy transfer rate based on dimensional analysis and an analogy with the “return-to-isotropy” evolution of RS anisotropy. This form includes two uncertain parameters that control the CS-ST interaction.

We present results for three different flow configurations: flow over a circular cylinder, flow over a square cylinder, and flow through a pin-fin array. In all cases, the model performance will be quantified by comparing results for the mean velocity and turbulence kinetic energy obtained from a set of simulations with the proposed model, using different values for the uncertain parameters, to reference data available from experiments or large eddy simulations (LES). In addition, results from a baseline RANS model, and from a RANS simulation with RS shape perturbations (RSSP) towards the one-component limit, are included for comparison.

The remainder of this paper first introduces the formulation of the conceptual model in Sec. II. Subsequently, we present the three test cases and their results in Sec. III. To conclude, Sec. IV provides a summary and suggestions for further model improvements.

## II. DSDL MODEL FORMULATION

In this section, we first introduce the double-scale concept and the transport equations for CS and ST energy. Subsequently, we present how the LEV assumption is employed for the CS and ST stress, respectively, resulting in a semiclosed form for the DSDL model with the energy transfer rate unknown. Lastly, we introduce the parametrization of the energy transfer between CS and ST with two uncertain parameters. Throughout this section, we consider an incompressible flow with constant density  $\rho$  and kinetic viscosity  $\nu$ .

## A. The double-scale concept

### 1. Triple decomposition

The proposed framework uses the triple decomposition concept [41] from unsteady-RANS to decompose instantaneous variables such as the velocity  $u_i$  into contributions from the mean field, coherent structures, and stochastic turbulence:

$$u_i = U_i + u_i^c + u_i^s. \quad (1)$$

In Eq. (1),  $U_i \equiv \bar{u}_i$ ,  $u_i^c \equiv \tilde{u}_i - \bar{u}_i$ , and  $u_i^s \equiv u_i - \tilde{u}_i$ , where  $\bar{u}_i$  and  $\tilde{u}_i$  are the long-time, i.e., considerably longer than the timescale of CS, and short-time, i.e., considerably longer than the timescale of ST but smaller than that of CS, averages, respectively. The total velocity fluctuation is defined as  $u_i' \equiv u_i^c + u_i^s = u_i - U_i$ . Furthermore, we assume that any long-time cross correlation between  $u_i^c$  and  $u_i^s$  (e.g.,  $\overline{u_i^c u_j^s}$  or  $\overline{u_i^c u_j^s u_k^c}$ ) vanishes. Thus, the model's ultimate output, i.e., the total RS  $\overline{u_i' u_j'}$  that is to affect the mean momentum transport, is equal to the sum  $\overline{u_i^c u_j^c} + \overline{u_i^s u_j^s}$ .

### 2. Transport equations for CS and ST energy

The kinetic energy of total fluctuations  $k \equiv \overline{u_i' u_i'}/2$  is the summation of CS energy  $k^c \equiv \overline{u_i^c u_i^c}/2$  and ST energy  $k^s \equiv \overline{u_i^s u_i^s}/2$ . We can derive the exact transport equations for  $k^c$  and  $k^s$ , respectively, as

$$\bar{D}_t k^c = \mathcal{P}^c - \zeta - \varepsilon^c + \mathcal{D}^c, \quad (2a)$$

$$\bar{D}_t k^s = \mathcal{P}^s + \zeta - \varepsilon^s + \mathcal{D}^s, \quad (2b)$$

where

$$\mathcal{P}^c \equiv -\overline{u_i^c u_j^c S_{ij}}, \quad \varepsilon^c \equiv \nu \overline{\frac{\partial u_i^c}{\partial x_j} \frac{\partial u_i^c}{\partial x_j}}, \quad \mathcal{D}^c \equiv \frac{\partial}{\partial x_i} \left( \nu \frac{\partial k^c}{\partial x_i} - \frac{1}{2} \overline{u_i^c u_j^c u_j^c} - \overline{u_i^c p^c} \right), \quad (3a)$$

$$\mathcal{P}^s \equiv -\overline{u_i^s u_j^s S_{ij}}, \quad \varepsilon^s \equiv \nu \overline{\frac{\partial u_i^s}{\partial x_j} \frac{\partial u_i^s}{\partial x_j}}, \quad \mathcal{D}^s \equiv \frac{\partial}{\partial x_i} \left( \nu \frac{\partial k^s}{\partial x_i} - \frac{1}{2} \overline{u_i^s u_j^s u_j^s} - \overline{u_i^s p^s} \right), \quad (3b)$$

$$\zeta \equiv -\overline{u_i^s u_j^s S_{ij}^c}. \quad (3c)$$

In Eqs. (2) and (3), the operator  $\bar{D}_t \equiv \partial_t + U_i \partial_i$  is the material derivative with respect to long time  $t$ , and thus equals  $U_i \partial_i$  in steady simulations;  $\mathcal{P}^{c/s}$ ,  $\varepsilon^{c/s}$ , and  $\mathcal{D}^{c/s}$  are the rates of production, dissipation, and diffusion of  $k^{c/s}$ , respectively; and  $S_{ij} \equiv (\partial_i U_j + \partial_j U_i)/2$  and  $S_{ij}^c \equiv (\partial_i u_j^c + \partial_j u_i^c)/2$  are the strain rates of the mean flow and of CS, respectively. The variable  $\zeta$ , which appears in both  $k^c$  and  $k^s$  equations but has opposite signs, is the spectral energy transfer rate from CS to ST. For high Reynolds numbers,  $\varepsilon^c$  is generally negligible compared to either  $\varepsilon^s$  or  $\zeta$ ; in this paper, we omit  $\varepsilon^c$ , and interpret  $\varepsilon^s$  as the overall energy dissipation rate, removing its superscript, i.e.,  $\varepsilon^c = 0$  and  $\varepsilon = \varepsilon^s$ .

Figure 1(b) provides a conceptual illustration of the dynamics for  $k^c$  and  $k^s$  using a ‘‘tank-tube’’ analogy. This analogy is similar to the sketch introduced by Hanjalic *et al.* [42] to illustrate their multiscale modeling concept; however, due to the formal introduction of two separate transport equations for  $k_c$  and  $k_s$  in this work, two additional phenomena are represented. First, we have an energy production  $\mathcal{P}^c$  or  $\mathcal{P}^s$  above each tank, indicating that the anisotropy of both CS and ST is considered; in Hanjalic *et al.* [42], the production is only injected into the largest scale. Second, we suppose the ‘‘tube’’ between the two ‘‘tanks’’ to have ‘‘inner roughness’’ and a ‘‘finite length,’’ which indicates the dependency of the energy transfer rate on the length scale separation between CS and ST (the reasoning is discussed in Sec. II C 1); the scale separation effect on the energy transfer is not explicitly considered in Hanjalic *et al.* [42].

## B. The double-LEV assumption

### 1. LEV assumption for ST stress

The ST stress  $\overline{u_i^s u_j^s}$  is closed using a conventional LEV model with

$$\overline{u_i^s u_j^s} = 2k^s \delta_{ij}/3 - 2\nu_t^s S_{ij}. \quad (4)$$

Using the standard  $k$ - $\varepsilon$  model [43] as an example, the eddy viscosity  $\nu_t^s$  in Eq. (4) is calculated from a dimensional argument,

$$\nu_t^s = C_\mu (k^s)^{1/2} l^s, \quad l^s \equiv (k^s)^{3/2}/\varepsilon. \quad (5)$$

Here,  $k^s$  is determined from solving the  $k^s$  equation (2 b) with a modeled diffusion term,

$$\mathcal{D}^s = \frac{\partial}{\partial x_i} \left[ \left( \nu + \frac{\nu_t^s}{\sigma_k} \right) \frac{\partial k^s}{\partial x_i} \right], \quad (6)$$

and a modeled  $\varepsilon$  equation,

$$\frac{\overline{D\varepsilon}}{\overline{Dt}} = \frac{\varepsilon}{k^s} [C_{\varepsilon 1}(\mathcal{P}^s + \zeta) - C_{\varepsilon 2} \varepsilon] + \frac{\partial}{\partial x_i} \left[ \left( \nu + \frac{\nu_t^s}{\sigma_\varepsilon} \right) \frac{\partial \varepsilon}{\partial x_i} \right]. \quad (7)$$

The constant  $C_\mu$  is equal to 0.09, and  $C_{\varepsilon 1}$ ,  $C_{\varepsilon 2}$ ,  $\sigma_k$ , and  $\sigma_\varepsilon$  are additional model-specific coefficients. Note that in Eq. (7), the dissipation is characterized by the ST timescale  $k^s/\varepsilon$  and the ‘‘production’’ is represented by  $\mathcal{P}^s + \zeta$  rather than  $\mathcal{P}^c + \mathcal{P}^s$ , consistent with the fact that the turbulent dissipation should not immediately respond to any large-scale motions.

### 2. LEV assumption for CS stress

For the CS stress  $\overline{u_i^c u_j^c}$ , we also assume an LEV form similar to Eqs. (4) and (5),

$$\overline{u_i^c u_j^c} = 2k^c \delta_{ij}/3 - 2\nu_t^c S_{ij}, \quad (8)$$

$$\nu_t^c = C_\mu (k^c)^{1/2} l^c, \quad (9)$$

as well as a modeled diffusion term in Eq. (2), which is similar to Eq. (6),

$$\mathcal{D}^c = \frac{\partial}{\partial x_i} \left[ \left( \nu + \frac{\nu_t^c}{\sigma_k} \right) \frac{\partial k^c}{\partial x_i} \right]. \quad (10)$$

However, different from the ST length scale  $l^s$ , the CS length scale  $l^c$  in Eq. (9) is not defined as  $(k^c)^{3/2}/\zeta$ . Since the initial stage of the CS generation is usually a highly nonequilibrium process with little dissipation or energy transfer towards small scales,  $\zeta$  should not be used to characterize  $l^c$ . Instead, we associate  $l^c$  with the mean flow field, as introduced in Sec. II B 3.

### 3. Estimation of CS length scale

Since the coherent structures of interest are associated with a specific mean flow pattern, it is natural to assume  $l^c$  to primarily scale with the mean flow length scale  $l^m$ , i.e.,  $l^c \sim l^m$ . To estimate  $l^m$ , we first consider a parallel shear flow, where the only nonzero component of the mean velocity gradient is  $\partial_y U_x$ . In this case,  $l^m$  can be estimated following Wilcox *et al.* [44],

$$l^m \sim |\partial_y U_x| / |\partial_{yy}^2 U_x|. \quad (11)$$

For general mean flows, we simply generalize Eq. (11) and define  $l^c$  as

$$l^c = c_m \Omega / \|\nabla S\|, \quad S \equiv \sqrt{2S_{ij}S_{ij}}, \quad \Omega \equiv \sqrt{2\Omega_{ij}\Omega_{ij}}, \quad (12)$$

where  $\Omega_{ij} \equiv (\partial_i U_j - \partial_j U_i)/2$  and  $c_m$  is a prefactor to be determined.  $l^c$  evaluated by Eq. (12) can be large near the center of a strong shear layer, where  $\Omega$  is large but  $\|\nabla S\|$  is small. In bluff body

flows, such a strong shear layer is generally induced by large flow separation and embeds vortex shedding, as shown in Fig. 1(c).

To select a plausible value of  $c_m$  in Eq. (12), we make the conceptual assumption that for a turbulent flow in local equilibrium, the calculated values of the effective eddy viscosity  $\nu_t = \nu_t^c + \nu_t^s$  should be identical under two circumstances: (a) all fluctuations are due to ST, i.e.,  $k = k^s$  and  $\nu_t = \nu_t^s$ , and (b) all fluctuations are due to CS, i.e.,  $k = k^c$  and  $\nu_t = \nu_t^c$ . If we take the log-layer in a boundary layer as an example of locally equilibrium turbulence, then this assumption results in the following relationship:

$$\kappa C_\mu^{1/4} k^{1/2} y = c_m C_\mu k^{1/2} y, \quad (13)$$

where  $\kappa \approx 0.41$  is the von Kármán constant. Equation (13) leads to

$$c_m = \kappa / C_\mu^{3/4} \approx 2.5. \quad (14)$$

Finally, in near-wall regions,  $l^c$  should also depend on the wall distance  $y$  and the friction length  $l_\tau \equiv \nu/u_\tau$ , where  $u_\tau$  is friction velocity on the wall. To represent these effects, we use the Baldwin-Lomax mixing length [45] as a limiter of  $l^c$ , yielding

$$l^c = (\kappa / C_\mu^{3/4}) \min\{\Omega / \|\nabla S\|, y [1 - \exp(-y^+ / A^+)]\}, \quad y^+ \equiv u_\tau y / \nu, \quad (15)$$

where  $A^+ \approx 26$  and  $u_\tau$  is locally approximated using the parallel shear flow relation  $u_\tau^2 \approx C_\mu^{1/2} k^s$ . Equation (15) will be used in Eq. (9) to calculate  $\nu_t^c$ .

### C. Modeling the CS-ST energy transfer

The three transport equations (2), (2b), and (7), combined with the two LEV relations (4) and (8), provide a three-equation, double-scale, double-LEV (DSDL) framework in semiclosed form. The only undetermined variable is the energy transfer rate  $\zeta$  between CS and ST. This section addresses the formulation of  $\zeta$ , which is a pivotal issue in the DSDL model development.

#### 1. Background and dimensional argument

Closing the interscale energy transfer rates is centered in most multiscale modeling concepts in general. One possible closing approach is to construct empirical transport equations through elaborate calibrations in diverse benchmark flows (e.g., Hanjalic *et al.* [42], Kim and Chen [46], Schiestel [47]). However, few studies have used this empirical approach to close the energy transfer rate from a specific type of CS to ST. Another approach is based on two-point closure theories, such as the Kovaszny hypothesis [48] adopted by Schiestel [49]; however, for turbulence with a significantly distorted spectrum by CS, the dimensional ground of the Kovaszny hypothesis is invalid. As such, we generally lack studies that directly inform the energy transfer rate modeling in a CS-ST system for steady-RANS simulations. We therefore design a simple conceptual model for the energy transfer rate  $\zeta$  for the UQ purpose, using a dimensional argument as a starting point.

The interaction between CS and ST generally tends to destruct the former while feeding the latter, i.e., it reduces  $k^c$  while increasing  $k^s$  at the rate of  $\zeta$ . Since this process is an intrinsic phenomenon of the dissipative system, we can infer that  $\zeta$  does not directly depend on external effects, e.g.,  $\mathcal{P}^c$  or  $\mathcal{P}^s$ ; instead, it only depends on the instantaneous characteristics of CS and ST themselves. Furthermore, informed by the definition (3), if we hypothesize that CS (or ST) can simply be characterized by their velocity scale ( $k^c$ )<sup>1/2</sup> [or ( $k^s$ )<sup>1/2</sup>] and their length scale  $l^c$  (or  $l^s$ ), then  $\zeta$  should be expressed as

$$\zeta = \zeta(k^c, l^c, k^s, l^s). \quad (16)$$

Using dimensional analysis, Eq. (16) can be rewritten as

$$\frac{\zeta}{(k^s)^{3/2} / l^s} = \frac{\zeta}{\varepsilon} = F\left(\frac{l^c}{l^s}, \frac{k^c}{k^s}\right), \quad (17)$$

with  $F$  a dimensionless function. Equation (17) indicates that  $\zeta$  primarily scales with  $\varepsilon$ , and that it depends on the length scale ratio  $l^c/l^s$  and the energy ratio  $k^c/k^s$ .

The dependence of  $F$  on  $k^c/k^s$  and  $l^c/l^s$  can be qualitatively informed by the tank-tube analogy from Fig. 1(b): a “higher pressure difference” (i.e., larger  $k^c/k^s$ ) or a “shorter tube length” (i.e., smaller  $l^c/l^s$ ) will yield a “larger flow rate” (i.e., larger  $\zeta$ ). Accordingly, we assume the following form for  $\zeta$ :

$$\zeta = f(l^c/l^s) g(k^c/k^s) \varepsilon, \quad (18)$$

in which  $g(k^c/k^s)$  is a nondecreasing function such that  $g(k^c/k^s) \varepsilon$  is the energy transfer rate when  $l^c/l^s = 1$ , and  $f(l^c/l^s)$  is a nonincreasing function representing the effect of length scale separation on the rate, with  $f(1) = 1$ . The functions  $g(k^c/k^s)$  and  $f(l^c/l^s)$  will be determined in Secs. II C 2 and II C 3, respectively.

## 2. An analogy with “return-to-isotropy”

To determine a plausible and concise form for  $\zeta = g(k^c/k^s) \varepsilon$  under the condition of no length scale separation (i.e.,  $l^c/l^s = 1$ ), we employ an analogy between the CS destruction process and a process in another nonequilibrium system—the “return-to-isotropy” (RI) process for an RS evolution [50].

First, consider an RS tensor in free-decaying turbulence. Assume the matrix form under its principal coordinate system to be

$$\mathbf{R} = \begin{bmatrix} \overline{u^2} & & \\ & \overline{v^2} & \\ & & \overline{w^2} \end{bmatrix}, \quad \overline{u^2} \geq \overline{v^2} \geq \overline{w^2}. \quad (19)$$

Its energy  $k = \text{tr}\{\mathbf{R}\}/2$  follows the equation

$$d_t k = -\varepsilon. \quad (20)$$

Now decompose  $\mathbf{R}$  into an anisotropic part  $\mathbf{R}^a$  and an isotropic part  $\mathbf{R}^b$ , where

$$\mathbf{R}^a = \begin{bmatrix} \overline{u^2} - \overline{w^2} & & \\ & \overline{v^2} - \overline{w^2} & \\ & & 0 \end{bmatrix}, \quad \mathbf{R}^b = \begin{bmatrix} \overline{w^2} & & \\ & \overline{w^2} & \\ & & \overline{w^2} \end{bmatrix}. \quad (21)$$

According to the (linear) RI theory and the isotropic dissipation assumption, the evolution of  $\mathbf{R}^a$  is governed by

$$d_t \mathbf{R}^a = -C_{\text{RI}} (\varepsilon/k) \mathbf{R}^a, \quad C_{\text{RI}} = 1.5 \sim 1.8. \quad (22)$$

Thus, the “energy” contained in  $\mathbf{R}^a$ ,  $k^a = \text{tr}\{\mathbf{R}^a\}/2$ , follows the equation

$$d_t k^a = -C_{\text{RI}} (\varepsilon/k) k^a. \quad (23)$$

Combining Eqs. (20) and (23) results in the equation for the energy fraction  $k^a/k$ ,

$$d_t (k^a/k) = -(C_{\text{RI}} - 1) (\varepsilon/k) (k^a/k). \quad (24)$$

Equation (24) basically reflects the RI process in which a nonequilibrium state (i.e., anisotropy or  $k^a/k > 0$ ) spontaneously tends towards an equilibrium state (i.e., isotropy or  $k^a/k = 0$ ); this process is characterized by the timescale proportional to  $k/\varepsilon$ .

Next, we draw an analogy between the energy  $k^a$  and  $k^b$  contained in an RS and the energy  $k^c$  and  $k^s$  in a CS-ST system, respectively. On one hand, the equation for the energy fraction  $k^c/k$  can be obtained from Eq. (2) with negligible production and diffusion,

$$d_t (k^c/k) = -(\varepsilon/k) (\zeta/\varepsilon - k^c/k), \quad (25)$$

TABLE I. Summary of DSDL model formulation.

Total RS	$\overline{u_i^c u_j^c} = \overline{u_i^c} \overline{u_j^c} + \overline{u_i^s u_j^s};$
CS stress	$\overline{u_i^c u_j^c} = 2k^c \delta_{ij}/3 - 2\nu_i^c S_{ij}, \quad \nu_i^c = C_\mu (k^c)^{1/2} l^c,$ $l^c = (\kappa/C_\mu^{3/4}) \min\{\Omega/\ \nabla S\ , y(1 - e^{-y^+/A^+})\}, \quad y^+ = C_\mu^{1/4} (k^s)^{1/2} y/\nu,$ $\overline{D}_i k^c = \mathcal{P}^c - \zeta + \partial_i[(\nu + \nu_i^c/\sigma_k)\partial_i k^c], \quad \mathcal{P}^c = -\overline{u_i^c u_j^c} S_{ij} (\Omega/S);$
ST stress	$\overline{u_i^s u_j^s} = 2k^s \delta_{ij}/3 - 2\nu_i^s S_{ij}, \quad \nu_i^s = C_\mu (k^s)^{1/2} l^s, \quad l^s = (k^s)^{3/2}/\varepsilon,$ $\overline{D}_i k^s = \mathcal{P}^s + \zeta - \varepsilon + \partial_i[(\nu + \nu_i^s/\sigma_k)\partial_i k^s], \quad \mathcal{P}^s = -\overline{u_i^s u_j^s} S_{ij} (\Omega/S),$ $\overline{D}_i \varepsilon = (\varepsilon/k^s)[C_{\varepsilon 1}(\mathcal{P}^s + \zeta) - C_{\varepsilon 2}\varepsilon] + \partial_i[(\nu + \nu_i^s/\sigma_\varepsilon)\partial_i \varepsilon];$
Energy transfer rate	$\zeta = C_{tr} f(l^c/l^s) (k^c/k) \varepsilon,$ $f(l^c/l^s) = \begin{cases} (1 + \tanh\{\alpha \ln[r_{1/2}/(l^c/l^s)]\})/2 & \text{if } l^c/l^s > 1, \\ 1 & \text{if } l^c/l^s \leq 1, \end{cases} \quad \alpha = 5.0,$ with uncertain parameters $C_{tr} \in (1, \infty)$ and $r_{1/2} \in (1, \infty)$ .

while on the other hand, we assume a “return-to-ST” process in which  $k^c/k$  behaves similarly to  $k^a/k$  and is governed by Eq. (24), i.e.,

$$d_t(k^c/k) = -(C_{tr} - 1)(\varepsilon/k)(k^c/k), \quad (26)$$

where the coefficient  $C_{tr} \in (1, \infty)$  controlling the CS-ST energy transfer is a counterpart of the coefficient  $C_{RI}$  controlling the RI process. Equations (25) and (26) result in

$$\zeta = C_{tr} (k^c/k) \varepsilon. \quad (27)$$

This simple form indicates that  $\zeta$  scales with  $\varepsilon$  and is driven by the energy proportion  $k^c/k$ , which is consistent with the qualitative analysis in Sec. II C 1. The coefficient  $C_{tr} \in (1, \infty)$  can be regarded as an indicator of the “cross-section area” of the tube between the two tanks in Fig. 1(b).

### 3. Effect of length scale separation

Based on the analysis of the length scale separation effect in Sec. II C 1, we hypothesize the following properties that a desired model function  $f(l^c/l^s)$  should have:

- (i)  $f(l^c/l^s)$  is nonincreasing for any  $l^c/l^s > 0$ ;
- (ii)  $f(l^c/l^s) = 1$  for  $l^c/l^s \leq 1$ ;
- (iii)  $f(l^c/l^s) \rightarrow 0$  as  $l^c/l^s \rightarrow \infty$ .

Accordingly and for simplicity, a smoothed step function as shown in Fig. 1(d) is selected,

$$f(l^c/l^s) = \begin{cases} \frac{1}{2} \left[ 1 + \tanh \left( \alpha \ln \frac{r_{1/2}}{l^c/l^s} \right) \right] & \text{if } l^c/l^s > 1, \\ 1 & \text{if } l^c/l^s \leq 1. \end{cases} \quad (28)$$

In Eq. (28), the parameter  $r_{1/2} \in (1, \infty)$  represents the length scale ratio with which  $\zeta$  reduces to one-half of its value when  $l^c/l^s = 1$ .  $\alpha$  is a smoothing coefficient and set to be 5 in this paper due to the fact that varying  $\alpha$  in the range  $\sim 3$ –10 has little effect on the results. In Fig. 1(b),  $r_{1/2} \in (1, \infty)$  can be regarded as an indicator of the “inner roughness” of the tube between the two tanks, with a smaller  $r_{1/2}$  indicating a “rougher tube,” and vice versa.

## D. Summary and relation to conventional model

### 1. Summary of the model formulation

The DSDL model developed in Secs. II A–II C is summarized in Table I, using the standard  $k$ - $\varepsilon$  model to calculate the ST-related variables. We employ Kato’s correction [51] for the production terms  $\mathcal{P}^c$  and  $\mathcal{P}^s$  to avoid the “stagnation point anomaly” [52] that yields nonphysically high



energy production near upwind stagnation points. This correction would not be necessary if the wall-blocking effect on near-wall RS is accounted for separately in the baseline model. It would be straightforward to apply the DSDL concept to most other conventional single-scale, two-equation LEV models.

The uncertain parameters,  $C_{tr} \in (1, \infty)$  and  $r_{1/2} \in (1, \infty)$ , control the energy transfer rate in the DSDL model. A decrease of either tends to increase the system resistance to the CS-ST energy transfer process, thereby retarding the ST energy accumulation and the total energy dissipation. As both  $C_{tr}$  and  $r_{1/2}$  go to infinity, the energy transfer process becomes sufficiently fast to essentially prohibit any CS energy accumulation, and thus the conventional single-scale LEV model is recovered. The quantitative effects of the two parameters will be further investigated in Sec. III.

## 2. Relation to the conventional model

We conclude this section by further illustrating the relation between the conventional model and the DSDL model. The latter will be reformulated to facilitate the comparison, specifically under the condition of quasihomogeneity, i.e., with negligible diffusion terms.

First, it is straightforward that the sum of Eqs. (2) and (2b) is identical to the  $k$  equation of the conventional model,

$$\frac{\bar{D}k}{Dt} = \mathcal{P} - \varepsilon, \quad (29)$$

where  $\mathcal{P} = \mathcal{P}^c + \mathcal{P}^s$  is the production rate of the total energy  $k$ .

Second, Eqs. (5) and (9) for the eddy viscosity lead to

$$\frac{\mathcal{P}^s}{\mathcal{P}} = \frac{v_t^s}{v_t^s + v_t^c} = \frac{(k^s)^{1/2} l^s}{(k^s)^{1/2} l^s + (k^c)^{1/2} l^c} = \frac{1}{1 + (l^c/l^s)h}, \quad h \equiv (k^c/k^s)^{1/2}. \quad (30)$$

With Eq. (30) and the energy transfer rate form (18), the  $\varepsilon$  equation (7) can be formally rewritten as

$$\begin{aligned} \frac{\bar{D}\varepsilon}{Dt} &= \frac{\varepsilon}{k^s} [C_{\varepsilon 1}(\mathcal{P}^s + \zeta) - C_{\varepsilon 2} \varepsilon] \\ &= \frac{\varepsilon}{k} \frac{k}{k^s} \left\{ C_{\varepsilon 1} \left[ \mathcal{P} \frac{\mathcal{P}^s}{\mathcal{P}} + C_{tr} f(l^c/l^s) \frac{k^c}{k} \varepsilon \right] - C_{\varepsilon 2} \varepsilon \right\} \\ &= \frac{\varepsilon}{k} (C'_{\varepsilon 1} \mathcal{P} - C'_{\varepsilon 2} \varepsilon), \end{aligned} \quad (31)$$

which is identical to the conventional  $\varepsilon$  equation, except that the two coefficients are modified from  $C_{\varepsilon 1, \varepsilon 2}$  to  $C'_{\varepsilon 1, \varepsilon 2}$  via

$$\frac{C'_{\varepsilon 1}}{C_{\varepsilon 1}} = 1 + h^2 \left[ \frac{1 - (l^c/l^s)/h}{1 + (l^c/l^s)h} + C_{tr} f(l^c/l^s) \frac{\varepsilon}{\mathcal{P}} \right], \quad (32a)$$

$$\frac{C'_{\varepsilon 2}}{C_{\varepsilon 2}} = 1 + h^2. \quad (32b)$$

Equations (31) and (32) indicate that the introduction of the DSDL model is equivalent to injecting perturbation fields to the two coefficients that control the  $\varepsilon$  dynamics. The perturbation magnitudes are generally proportional to the local energy ratio  $h^2 = k^c/k^s$ .

On one hand, the perturbation to  $C_{\varepsilon 2}$  depends only on  $h$  and is always positive, thereby tending to accelerate the loss of  $\varepsilon$ . On the other hand, the perturbation to  $C_{\varepsilon 1}$  depends on additional local flow variables, including  $l^c/l^s$  and  $\mathcal{P}/\varepsilon$ , and can be either positive or negative. The effects of the  $C_{\varepsilon 1}$  perturbation may be partially illustrated by the following two properties:

(a) When  $h \ll 1$ , we have  $\frac{1 - (l^c/l^s)/h}{1 + (l^c/l^s)h} \simeq -(l^c/l^s)/h$ , so  $C'_{\varepsilon 1}/C_{\varepsilon 1} \simeq 1 - (l^c/l^s)h$ . It indicates that at the initial stage of  $k^c$  generation, the perturbation is negative and thus retards the increase of  $\varepsilon$ .

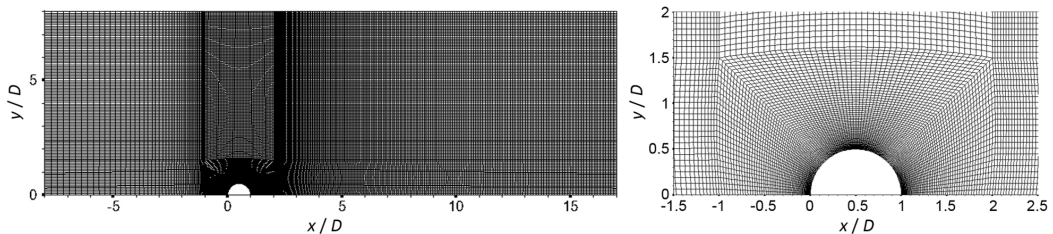


FIG. 2. Mesh for the case of flow past a circular cylinder. Left: in the entire domain; right: near the cylinder.

(b)  $C'_{\varepsilon_1}$  decreases monotonically with increasing  $l^c/l^s$ , and is asymptotic to zero as  $l^c/l^s \rightarrow \infty$ . This implies that a large length scale separation can force  $C'_{\varepsilon_1}$  to nearly vanish, thereby significantly retarding the increase of  $\varepsilon$ .

### III. RESULTS

In this section, the DSDL model developed in Sec. II is applied to three cases of bluff body flows. The low-Reynolds-number  $k$ - $\varepsilon$  model [53] and/or the Shear-stress-transport (SST)  $k$ - $\omega$  model [54] are used to calculate the ST-related variables. These models can be directly integrated to the walls without using extra wall functions, which are necessary for the standard  $k$ - $\varepsilon$  model.

For each case, three sets of steady-RANS simulations are implemented for comparison:

(1) BSL: one baseline simulation using a conventional single-scale LEV model [53,54].  
 (2) RSSP-1C(0.5): one simulation in which the RS shape predicted by the conventional model is perturbed halfway towards the one-component limit (i.e., the most efficient route to increase the local energy production rate,  $\mathcal{P}$ ) following the methodology in [15,22] (see the Appendix for a brief introduction of the RSSP method).

(3) DSDL( $C_{tr}$ ,  $r_{1/2}$ ): a set of simulations in which the DSDL model (using the conventional model to calculate ST-related variables) is applied for various values of  $C_{tr}$  and  $r_{1/2}$ .

Note that Kato's production correction [51], i.e.,  $\mathcal{P} = -\overline{u'_i u'_j} S_{ij} (\Omega/S)$ , is also applied in the BSL and RSSP-1C simulations.

All simulations are implemented using the open-source software OPENFOAM [55]. The differential equations are spatially discretized using the second-order finite-volume method. The SIMPLE algorithm is adopted for pressure-velocity decoupling. The solution is considered to be converged when the global residuals of momentum and energy decrease more than four orders of magnitude and the QoIs reach their steady-state values. The near-wall grid resolutions are high enough to ensure  $\Delta y^+ \leq 1$ , avoiding the use of wall functions. For each case, the results presented in this section were demonstrated to be grid independent by performing simulations with a finer mesh (resolution  $\sim 25$ – $30\%$  higher in each dimension) and verifying that discrepancies between the QoIs predicted by both meshes were smaller than 1%.

#### A. Flow past a circular cylinder

The first test case considers the flow past a circular cylinder of infinite length with cross-section diameter  $D$ . Reference data is available from an experiment in Lourenco and Shih [56] and LES (“Run C2”) in Breuer [57]. The Reynolds number  $Re = U_\infty D/\nu$  is 3900, where  $U_\infty$  is the free stream velocity. Figure 2 depicts the two-dimensional computational domain, which is discretized using around 39 600 cells. The simulations employ symmetric boundary conditions at  $y/D = 0$  and  $y/D = 8$ . To match to flow conditions from the experiments and LES, we impose a uniform free stream velocity with a turbulence intensity  $Tu = \sqrt{2k/3}/U_\infty$  of 0.1% at the inflow boundary ( $x/D = 8$ ). Assuming that no CS exist at the inflow, we set  $k^c/k = O(10^{-6})$  at the inlet. The outlet boundary is placed at  $x/D = 17$ , with zero-gradient conditions for  $U_i$ ,  $k^c$ ,  $k^s$ , and  $\varepsilon$  (or  $\omega$ ).

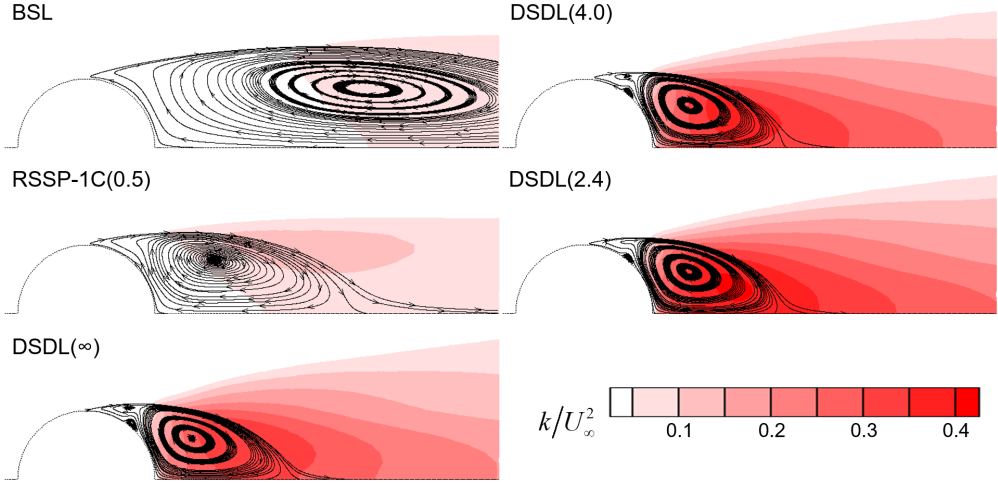


FIG. 3. Mean streamlines and total fluctuation energy contours around the recirculation region behind the circular cylinder (using the  $k$ - $\omega$  SST model as the baseline).  $C_{tr} = 1.5$  for DSDL simulations.

### 1. Results for varying $r_{1/2}$

We first investigate the length scale separation effect on the DSDL model by varying  $r_{1/2}$  while fixing  $C_{tr}$ . The latter is selected to be 1.5, similar to the RI coefficient  $C_{RI}$  in Eq. (22).

Figure 3 visualizes the recirculation regions and the total fluctuation energy predicted by the three sets of steady-RANS simulations. The BSL predicts an excessively long recirculation region, while the increased turbulence kinetic energy in the RSSP-1C and DSDL reduces the wake regions to around  $1D$ . The value for  $r_{1/2}$  is found to have a limited influence on the mean velocity field predicted by the DSDL, but it does affect the turbulence kinetic energy in the wake region. As expected, decreasing  $r_{1/2}$ , which decreases the energy transfer rate, results in an increase in the overall level of turbulence.

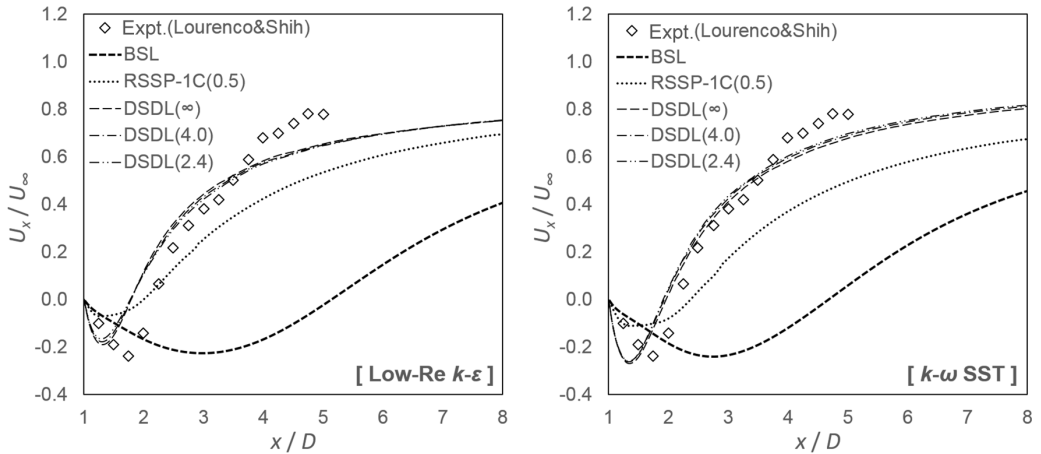


FIG. 4. Distributions of mean velocity component  $U_x$  along the center line  $y = 0$  downstream of the circular cylinder. (Left: using the low-Re  $k$ - $\varepsilon$  model as baseline; right: using the  $k$ - $\omega$  SST model as the baseline. Same for Figs. 5, 10, and 11.)  $C_{tr} = 1.5$  for DSDL simulations.

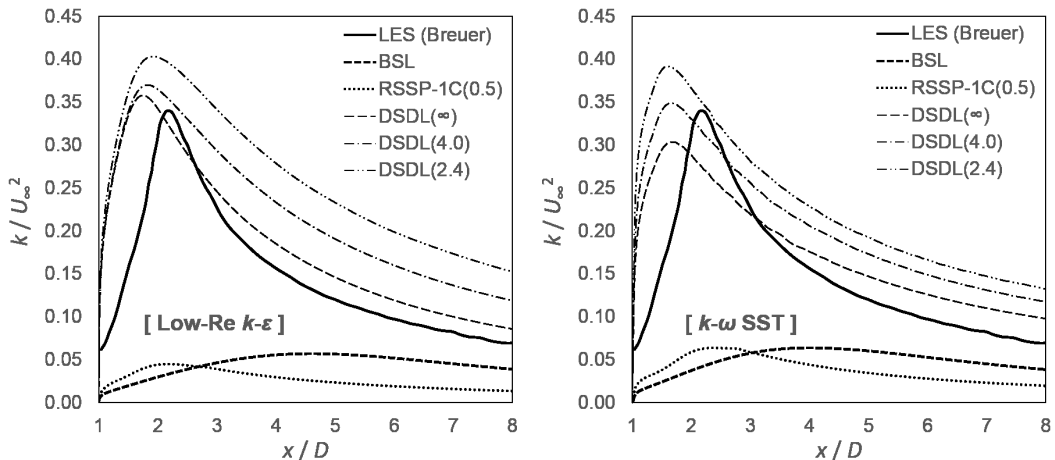


FIG. 5. Distributions of total fluctuation energy  $k$  along the center line  $y = 0$  downstream of the circular cylinder.  $C_{tr} = 1.5$  for DSDL simulations.

Figures 4 and 5 present a quantitative comparison of the simulations and the reference data by plotting the mean velocity and turbulence kinetic energy profiles along the center line  $y = 0$ . For the mean velocity prediction, both the RSSP-1C and the DSDL significantly reduce the discrepancies with the experimental data observed in the BSL result; overall, the DSDL velocity prediction, which shows negligible dependency on  $r_{1/2}$ , provides the best agreement with the experiment.

The turbulence kinetic energy profiles (Fig. 5) further demonstrate the superiority of the DSDL over both the BSL and RSSP-1C. The BSL and RSSP-1C significantly underestimate the energy levels downstream of the cylinder; the peak value discrepancies with the LES data are  $\sim -87\%$ – $-83\%$ . The DSDL model significantly reduces the discrepancies in both the profile shapes and the peak values: for the uncertain parameter  $r_{1/2}$  decreasing from  $\infty$  to 2.4, the peak value discrepancies vary from  $+4\%$  to  $+18\%$  (with low-Re  $k-\varepsilon$  as the baseline) or from  $-11\%$  to  $+14\%$  (with  $k-\omega$  SST as the baseline). Compared to the mean velocity, the turbulence kinetic energy depends more strongly on  $r_{1/2}$ . Simulations considering the full range of possible values ( $r_{1/2} \in [1, +\infty)$ ) would result in large uncertain intervals for the prediction of the turbulence kinetic energy. However, adequate calibration can be expected to improve the predictive capabilities; based on the current analysis, the interval  $r_{1/2} \in [2.4, +\infty)$  is recommended for the case of flow over circular cross sections.

To further investigate the mechanisms that cause the increased energy levels predicted by the DSDL method, Fig. 6 provides contour plots of the scale ratio and the CS energy production rate. As expected, large-scale ratios  $l^c/l^s$  exist around the border between the wake downstream of the cylinder and the outer main flow region; these large ratios suppress the energy transfer from  $k^c$  to  $k^s$ . At the same time, there is intense production of  $k^c$  in this region. The resulting locally high

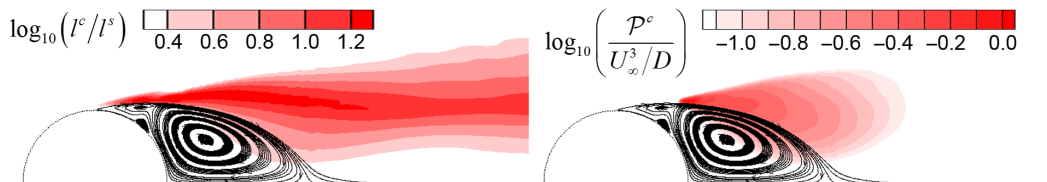


FIG. 6. Logarithmic contours of scale ratio  $l^c/l^s$  (left) and CS energy production rate  $\mathcal{P}^c$  (right) behind the circular cylinder. Simulation DSDL with  $C_{tr} = 1.5$  and  $r_{1/2} \rightarrow \infty$ ; using the  $k-\omega$  SST model as the baseline.

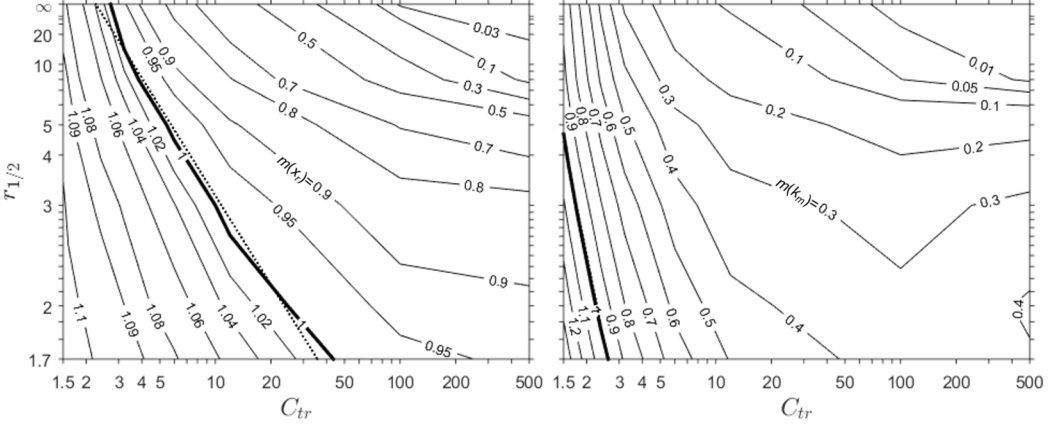


FIG. 7. Isolines of the metrics  $m(x_r)$  (left) and  $m(k_m)$  (right) with respect to parameters  $C_{tr}$  and  $r_{1/2}$  for the case of a circular cylinder (using the  $k$ - $\omega$  SST model as the baseline). The axes of  $C_{tr}$  and  $r_{1/2}$ , respectively, use a logarithmic scale and a reciprocal scale, under which the isolines  $m(\cdot) = 1$  are linearly fitted by the dashed lines.

level of  $k^c$  is subsequently transported via both the (modeled) turbulent diffusion and the mean flow convection to the region near the center line.

## 2. Results for varying $C_{tr}$ and $r_{1/2}$

The results in Sec. III A 1 indicate that given  $C_{tr} = 1.5 \approx C_{RI}$ , the DSDL model with  $r_{1/2} \in [2.4, \infty)$  achieves reasonable agreement with the reference data in terms of the size and the energy level of the recirculation zone. In the following, we further relax the condition  $C_{tr} \approx C_{RI}$  and investigate the predictions in the recirculation zone for jointly varying  $C_{tr}$  and  $r_{1/2}$ . To support this investigation, we define two metrics that represent the improvement in the DSDL predictions for the size and the energy level of the recirculation zone compared to the BSL prediction.

On the center line  $y = 0$  downstream of the cylinder, denote the  $x$  coordinate where the mean velocity  $U_x$  is zero by  $x_r$  and the maximum value of total fluctuation energy  $k$  by  $k_m$ .  $x_r$  and  $k_m$  are used to characterize the size and the energy level of the recirculation zone. Further define two metrics  $m(x_r)$  and  $m(k_m)$  as

$$m(x_r) = (x_r - x_r|_{BSL}) / (x_r|_{REF} - x_r|_{BSL}), \quad (33a)$$

$$m(k_m) = (k_m - k_m|_{BSL}) / (k_m|_{REF} - k_m|_{BSL}), \quad (33b)$$

where  $\cdot|_{REF}$  and  $\cdot|_{BSL}$  represent the quantities resulting from the reference data (by LES or experiments) and from the BSL simulation, respectively. Accordingly, the proximity of  $m(\cdot)$  to a value of 1 represents the DSDL model's capability to improve upon the BSL model prediction.

We select the values of  $C_{tr}$  from the set  $\{1.5, 1.6, 1.8, 2.4, 3.2, 6.0, 12, 100, 500\}$  and  $r_{1/2}$  from  $\{1.7, 2, 3, 5, 8, \infty\}$ , and implement  $9 \times 6 = 54$  DSDL simulations. The resulting isolines of  $m(x_r)$  and  $m(k_m)$  are plotted in Fig. 7 with respect to  $C_{tr}$  and  $r_{1/2}$ . The figure shows that both  $m(x_r)$  and  $m(k_m)$  are asymptotic to zero as  $C_{tr}$  and  $r_{1/2}$  simultaneously approach infinity, which is consistent with the discussion in Sec. II D. As either  $C_{tr}$  or  $r_{1/2}$  decreases, both  $m(x_r)$  and  $m(k_m)$  generally tend to increase. A total consistency with the reference data is realized on the isolines with  $m(\cdot) = 1$ , which can be approximated by the fitted relations  $\log_{10}(C_{tr}/2.25) = 2.04/r_{1/2}$  for  $m(x_r) = 1$  and  $\log_{10}(C_{tr}/1.06) = 0.66/r_{1/2}$  for  $m(k_m) = 1$ . For  $1.5 \leq C_{tr} \lesssim 10$ , the variation in  $m(x_r)$  is generally small, within the range of  $\sim 0.9$ – $1.1$ .  $m(k_m)$  is much more sensitive to either parameter, varying within the range of  $\sim 0.3$ – $1.3$ . When  $C_{tr} = 1.5$  and  $2.4 \leq r_{1/2} < \infty$ , as suggested in Sec. III A 1, we

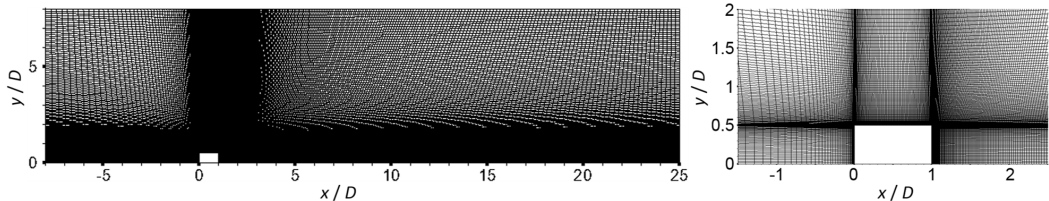


FIG. 8. Mesh for the case of flow past a square cylinder. Left: in the entire domain; right: around the cylinder.

have  $m(x_r) \sim 1.08\text{--}1.10$  and  $m(k_m) \sim 0.85\text{--}1.15$ . Similar ranges of  $m(x_r)$  and  $m(k_m)$  can be realized when  $C_{tr}$  and  $r_{1/2}$  follow the relation  $\log_{10}(C_{tr}/a) = 0.66/r_{1/2}$  with  $a \sim 0.8\text{--}1.5$ .

In summary, Fig. 7 demonstrates that reasonable predictions of both the size and the energy level of the recirculation zone approximately require  $C_{tr} \lesssim 4$ . This implies that  $C_{tr}$ , if regarded as a quasi-universal coefficient in similar flow configurations, is indeed not too far from the common range of the return-to-isotropy coefficient  $C_{RI}$ .

## B. Flow past a square cylinder

The second test case considers the flow past a square cylinder of infinite length with cross-section side length  $D$ . Reference data is available from an experiment [58] at  $Re = U_\infty D/\nu = 14\,000$ . Figure 8 shows the computational domain, which is discretized using around 64 000 cells. The boundary conditions are set similarly to the circular cylinder case, except that  $Tu = 6\%$  at the inlet.

### 1. Results for varying $r_{1/2}$

As in Sec. III A 1, we first discuss the  $r_{1/2}$  effect under a fixed  $C_{tr} = 1.5$ . Figure 9 shows the predictions for the mean flow and turbulence kinetic energy in the recirculation region. Similarly to

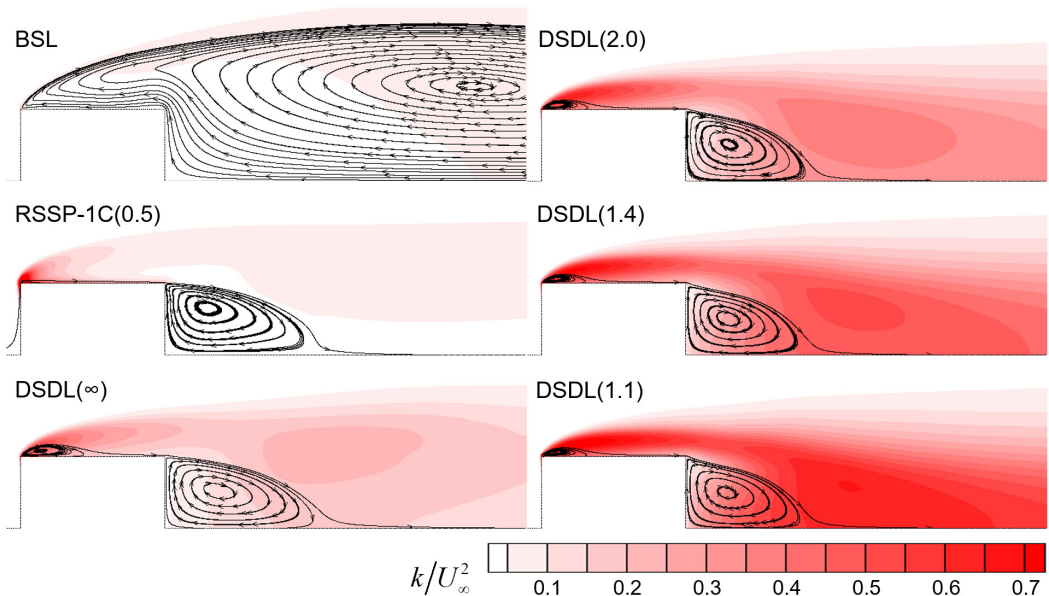


FIG. 9. Mean streamlines and total fluctuation energy contours around the recirculation region behind the square cylinder (using the low- $Re$   $k$ - $\varepsilon$  model as the baseline).  $C_{tr} = 1.5$  for DSDL simulations.

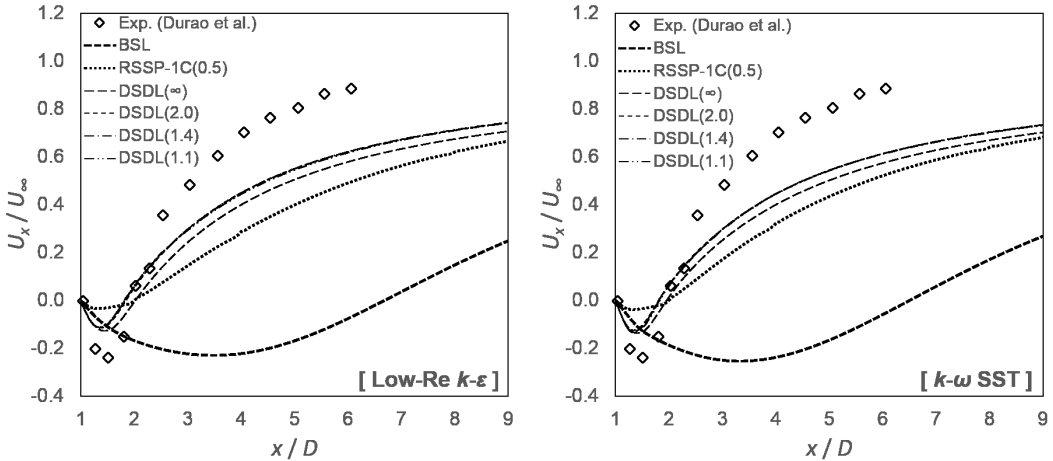


FIG. 10. Distributions of mean velocity component  $U_x$  along the center line  $y = 0$  downstream of the square cylinder.  $C_{tr} = 1.5$  for DSDL simulations.

the case in Sec. III A, the recirculation region predicted by the BSL is excessively large. In addition, the flow on the side wall of the cylinder never reattaches. In contrast, the RSSP-1C and DSDL predict recirculation lengths of around  $1D$ , in combination with a small separation bubble on the side wall. The differences in the mean flow are combined with higher predicted turbulence kinetic energies around the edges of the separation zones. As for the circular cylinder, the value for  $r_{1/2}$  has a limited influence on the mean velocity field predicted by the DSDL, but it does significantly affect the turbulence kinetic energy.

Figures 10 and 11 present a quantitative comparison of the simulations and the reference data by plotting the mean velocity and turbulence kinetic energy profiles along the center line  $y = 0$ . For the mean velocity, the results demonstrate that the RSSP-1C and the DSDL provide a significantly improved prediction compared to the BSL result.

Considering the turbulence kinetic energy, the BSL and RSSP-1C underestimate the energy level more strongly than for the circular cylinder: the discrepancies with the experimental peak

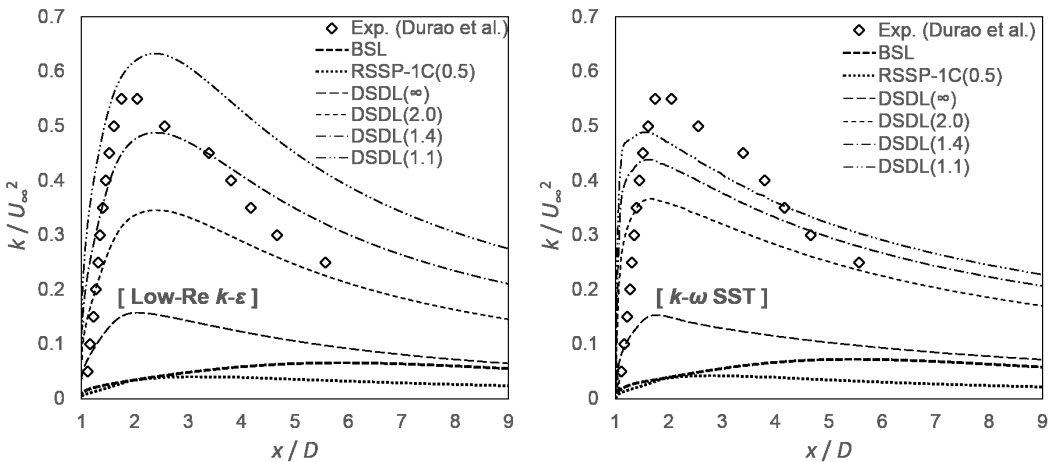


FIG. 11. Distributions of total fluctuation energy  $k$  along the center line  $y = 0$  downstream of the square cylinder.  $C_{tr} = 1.5$  for DSDL simulations.

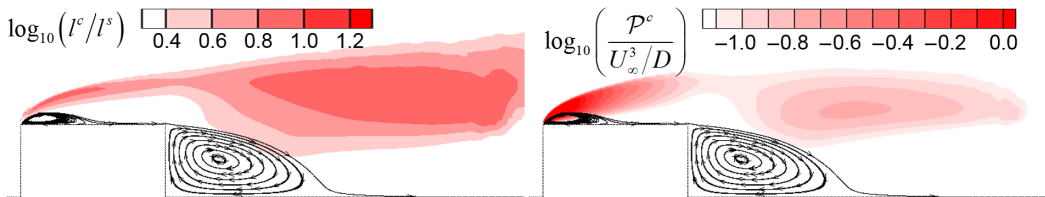


FIG. 12. Logarithmic contours of the scale ratio  $l^c/l^s$  (left) and CS energy production rate  $\mathcal{P}^c$  (right) behind the square cylinder. Simulation DSDL with  $C_{tr} = 1.5$  and  $r_{1/2} \rightarrow \infty$ ; using the low-Re  $k-\varepsilon$  model as the baseline.

values are  $\sim -93\%$ – $-88\%$ . This discrepancy is moderately decreased to  $-72\%$  when using the DSDL method with infinite  $r_{1/2}$ ; for values as low as 1.4 to 1.1, the discrepancy is reduced more significantly to  $-13\%$  to  $+13\%$  with the low-Re  $k-\varepsilon$  as the baseline or from  $-22\%$  to  $-12\%$  with the  $k-\omega$  SST as the baseline. The plots confirm the previously observed strong dependency of the turbulence kinetic energy on  $r_{1/2}$ . Calibration of this parameter can support reducing the prediction intervals for the energy levels; based on the current analysis, we recommend the interval  $r_{1/2} \in [1.1, 1.4]$  for the case of flow over bodies with square cross sections.

Figure 12 depicts the contour plots of the scale ratio and the CS energy production rate to further investigate the mechanisms that cause the increased energy levels predicted by the DSDL method. Different from Fig. 6, large  $l^c/l^s$  exist in two regions around the square cylinder: a more narrow region is associated with the front-corner separation, while a wider region exists along the border between the wake region and the outer mean flow. These regions support the transport of locally generated turbulence downstream along the side wall and towards the center line via both the (modeled) turbulent diffusion and the mean flow convection.

## 2. Results for varying $C_{tr}$ and $r_{1/2}$

In the following, we apply the same procedure as in Sec. III A 2 to investigate the dependence of the recirculation zone characteristics on both parameters  $C_{tr}$  and  $r_{1/2}$ . The set of  $C_{tr}$  values is  $\{1.4, 1.5, 1.8, 2.4, 3.6, 6.0, 20, 100, 1000\}$  and the set of  $r_{1/2}$  values is  $\{1.1, 1.4, 2.0, 5.0, \infty\}$ , yielding  $9 \times 5 = 45$  DSDL simulations.

Figure 13 shows isolines of the metrics  $m(x_r)$  and  $m(k_m)$  with respect to  $C_{tr}$  and  $r_{1/2}$ . Similar trends as in Fig. 7 are observed in terms of the asymptotic behaviors, the joint monotonicity, and the difference in sensitivity between  $m(x_r)$  and  $m(k_m)$ . A characteristic of Fig. 13 that is different from Fig. 7 is that smaller values for both  $C_{tr}$  and  $r_{1/2}$  are needed to achieve  $m(\cdot) = 1$ ; the fitted relations for  $m(x_r) = 1$  and  $m(k_m) = 1$  are  $\log_{10}(C_{tr}/0.68) = 1.34/r_{1/2}$  and  $\log_{10}(C_{tr}/0.70) = 0.41/r_{1/2}$ , respectively. The parameter values  $C_{tr} = 1.5$  and  $1.1 \leq r_{1/2} \leq 1.4$  recommended in Sec. III B 1 correspond to  $m(x_r) \approx 1.03$  and  $m(k_m) \sim 0.85$ – $1.15$ . The same ranges of  $m(x_r)$  and  $m(k_m)$  can also be approximately realized when  $C_{tr}$  and  $r_{1/2}$  follow the relation  $\log_{10}(C_{tr}/a) = 0.41/r_{1/2}$  with  $a \sim 0.65$ – $0.75$ .

Similarly to the summary in Sec. III A 2, Fig. 7 demonstrates that reasonable predictions of both the size and the energy level of the recirculation zone require  $C_{tr} \lesssim 2$ . This further confirms that appropriate values of  $C_{tr}$  are within or close to the common range for  $C_{RI}$ .

## C. Flow in a pin-fin array

The third test case considers the flow in a pin-fin array consisting of eight staggered rows of circular cylinders (pins) placed between two parallel flat plates (fins). This case was first studied experimentally by Ames *et al.* [59], followed by several numerical studies including a high-fidelity LES reported by Hao and Gorlé [60]. We will use the validated LES results presented in [60] as the reference data in this paper. Figure 14 shows the computational domain, ranging over one-half



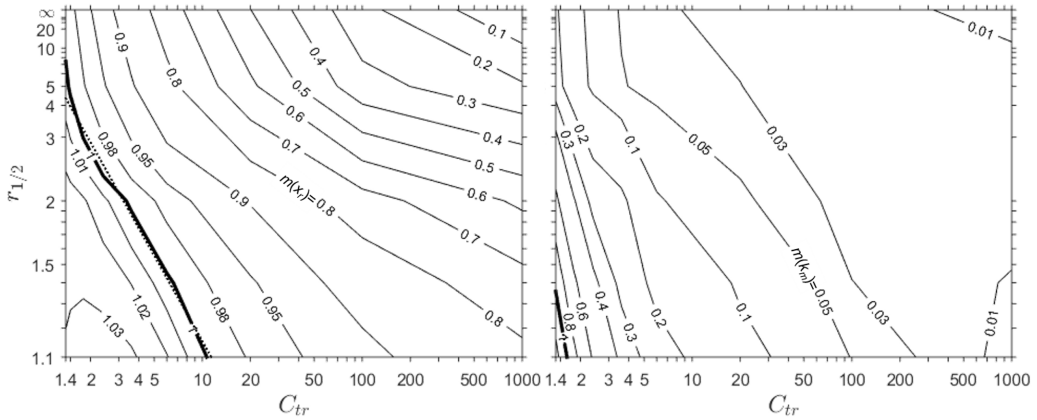


FIG. 13. Isolines of the improvement functions  $m(x_r)$  (left) and  $m(k_m)$  (right) with respect to parameters  $C_{tr}$  and  $r_{1/2}$  for the case of a square cylinder (using the low-Re  $k-\varepsilon$  model as the baseline). The axes of  $C_{tr}$  and  $r_{1/2}$ , respectively, use a logarithmic scale and a reciprocal scale, under which the isolines  $m = 1$  are linearly fitted by the dashed lines.

of the lateral ( $y$ ) pin spacing and one-half of the fin spacing due to symmetries. The Reynolds number  $Re = V_m D / \nu = 10\,000$ , where  $D$  is the diameter of the cylindrical pins and  $V_m$  is the average velocity on the throat cross section between two laterally adjacent pins. The entire computational domain is discretized using about 2 650 000 cells. More details on the simulation setup can be found in Hao and Górlé [22]. The  $k-\omega$  SST model is used as the baseline model. Based on the suggestion for the case of flow over the circular cylinder in Sec. III A, we use  $C_{tr} = 1.5$  and  $r_{1/2} \in [2.4, +\infty)$  for this configuration with multiple circular cylinders.

Figure 15 displays the recirculation region and the total fluctuation energy predictions behind different pin rows. In the LES results, the recirculation region first decreases in size from rows 2 to 5, before becoming more constant on rows 5 to 7. The BSL predicted wake extents are larger and hardly change from rows 2 to 7. The results of RSSP-1C and DSDL are similar in terms

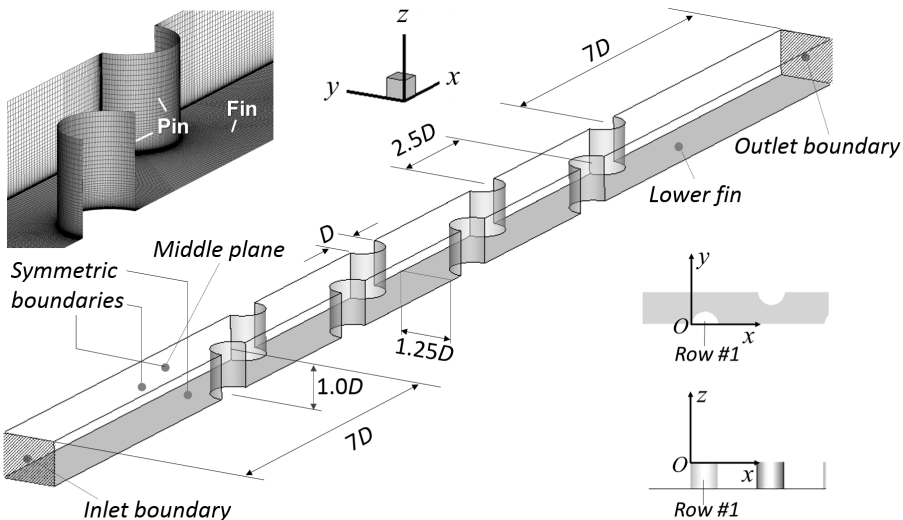


FIG. 14. Computational domain and mesh for the pin-fin array configuration.

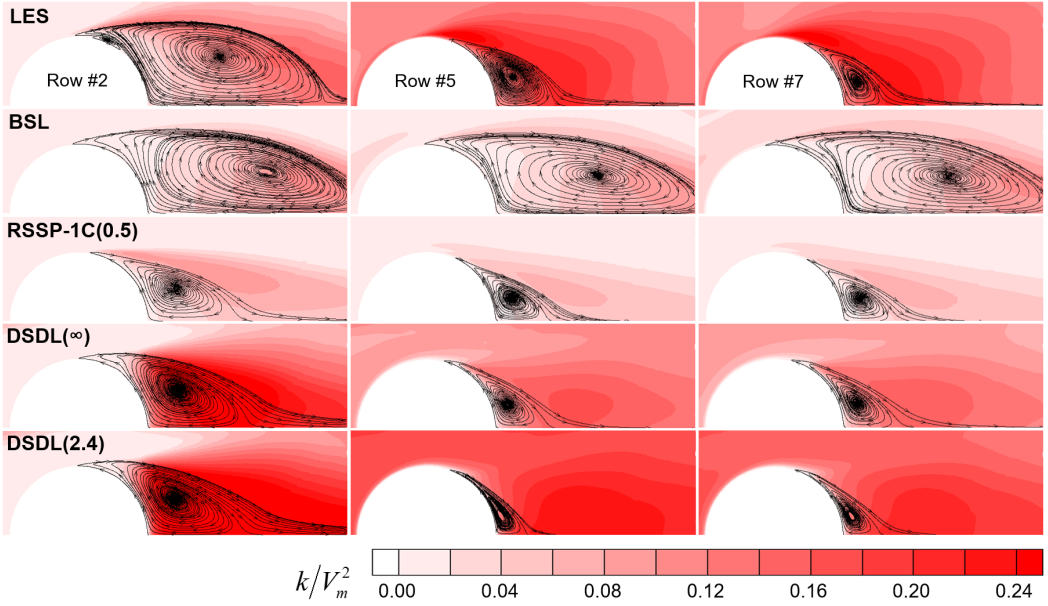


FIG. 15. Mean streamlines and total fluctuation energy contours on the center plane  $z = 0$  behind pin rows 2, 5, and 7 of the pin-fin array.  $C_{tr} = 1.5$  for DSDL simulations.

of the wake extents; relative to the LES, the predicted recirculation sizes are smaller for row 2, but comparable for rows 5 and 7. Considering the turbulence kinetic energy, the RSSP-1C has only a limited improvement over the baseline model; in contrast, the DSDL is far more capable of representing the levels of energy predicted by the LES.

Figures 16 and 17 show profiles of the mean velocity and turbulence kinetic energy along the center line  $y = 0$  on the center plane  $z = 0$ . Considering the mean velocity profile, the plot confirms the improved performance of the RSSP-1C and DSDL compared to the BSL in the fully developed flow regime (approximately from pin row 4 to 8). Considering the turbulence kinetic energy, Fig. 17 shows the significant energy underestimations by the BSL and RSSP-1C from row 3 to 8, while the DSDL results with  $r_{1/2} \in [2.4, +\infty)$  properly bound the majority of the LES data.

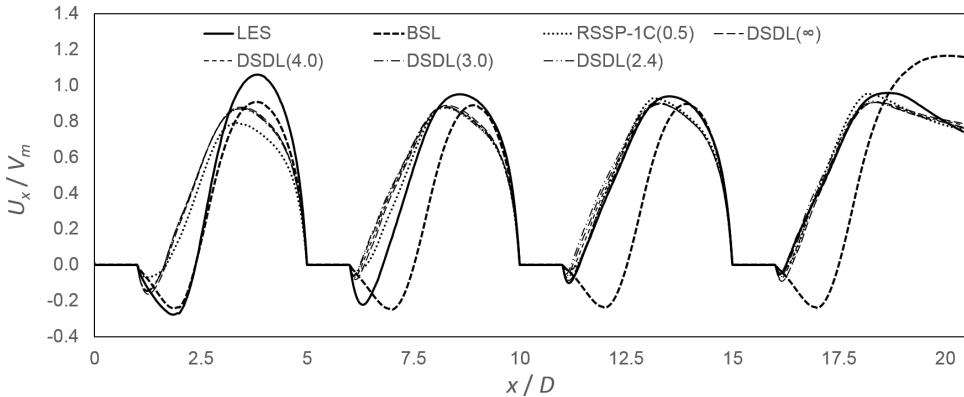


FIG. 16. Distributions of mean velocity component  $U_x$  along the center line  $y = 0$  on the center plane  $z = 0$  of the pin-fin array.

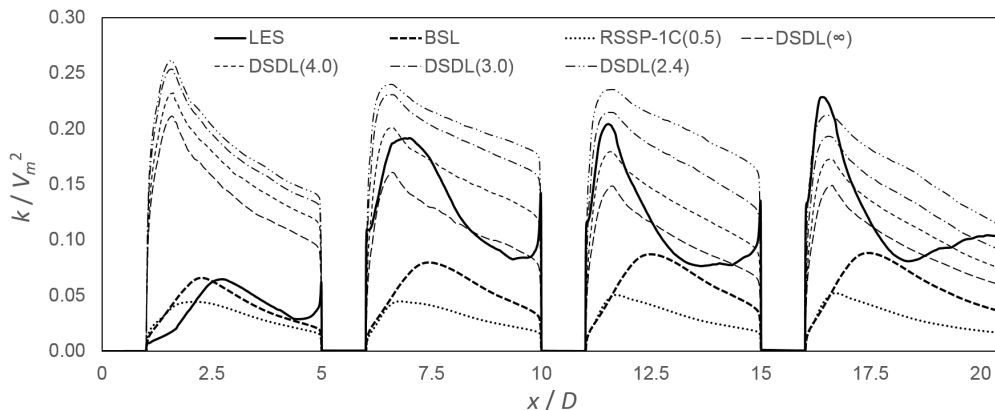


FIG. 17. Distributions of total fluctuation energy  $k$  along the center line  $y = 0$  on the center plane  $z = 0$  of the pin-fin array.

The most notable difference between the DSDL and the LES results is the slower energy decay process downstream of each energy peak in the DSDL. This inadequacy can primarily be attributed to the double-LEV assumption. Due to the geometry of this configuration, the flow downstream of a pin is subjected to a rapid contraction process as it approaches the throat cross section formed by the next row of pins. As indicated in a previous study of axisymmetric contraction flow in Lee and Reynolds [61], the RS cannot evolve synchronously with the mean strain rate during this rapid contraction; the real energy production rate is thus lower than that predicted by LEV assumption.

#### IV. CONCLUSIONS

In this paper, we present a conceptual model, termed the double-scale double-LEV (DSDL) model, to quantify uncertainty in the turbulence dissipation closure in steady-RANS simulations for flow past bluff bodies with vortex shedding. The model solves three transport equations, respectively, for the energy of coherent structures (CS), the energy of stochastic turbulence (ST), and the energy dissipation rate of ST. The energy transfer rate from CS to ST is modeled by an algebraic form with two uncertain parameters  $C_{tr} \in (1, \infty)$  and  $r_{1/2} \in (1, \infty)$  controlling the CS-ST interaction.

The DSDL model has been tested on the flow behind a circular and square cylinder of infinite length, and on the flow through a pin-fin array. For  $C_{tr}$  values similar to the common value of the “return-to-isotropy” coefficient  $C_{RI} \approx 1.5$ , the model significantly improves upon conventional two-equation LEV models [with or without RS shape perturbations (RSSP)], in terms of estimating the mean flow field and the fluctuation energy levels behind bluff bodies. The parameter  $r_{1/2}$  is found to have a limited influence on the mean flow, but a strong effect on the fluctuation energy. A reduction of  $r_{1/2}$  tends to amplify the scale separation effect and suppress the CS-ST energy transfer, resulting in a suppressed dissipation and an increase of the total fluctuation energy. The results for the flow configurations in this paper preliminarily suggest the intervals  $r_{1/2} \in [2.4, \infty)$  and  $r_{1/2} \in [1.1, 1.4]$  to be used for bluff bodies with circular cross sections and with square cross sections, respectively. In addition, the tests for varying  $C_{tr}$  values in this paper demonstrate that an appropriate value of  $C_{tr}$  for reasonably predicting both the sizes and the energy levels of the recirculation zones should be relatively close to the common value of  $C_{RI}$ .

To further improve the model performance, additional parameters, functional forms, and/or model structures in the proposed conceptual model could be relaxed and perturbed. First, different functional forms of the energy transfer rate, either revisiting  $f(l^c/l^s)$  and  $g(k^c/k^s)$  in Eq. (18) or incorporating more physics into Eq. (18) directly, could be explored. Second, the simple form

for the CS length scale determination in Eq. (12) should be evaluated for various flow patterns; methods to replace the algebraic expression for  $l^c$  by constructing transport equations for the length scales as in Schwarzkopf *et al.* [62] are worth exploring. Third, the constants  $C_\mu$  in Eqs. (5) and (9) could be revisited. A larger  $C_\mu$  in Eq. (9) than that in Eq. (5) could be considered to represent the general descending anisotropy of turbulence from large to small scales. Fourth, the properties of the model should be investigated in more diverse scenarios; in particular, discussions on its conformity to various physical constraints as summarized in Xiao and Cinnella [63] would be instructive to enhance the model's robustness. Last, the two LEV assumptions, and especially that for CS, might have to be perturbed. For example, both the shape and orientation of the RS related to CS could be perturbed to reflect the quasi-two-dimensional nature of vortex shedding. One could also comprehensively explore combining the proposed model with perturbations to the RS shape and/or orientation. This exploration, which could be aided by various data-driven techniques, could generate new insights on the relative importance of uncertainty introduced by the LEV assumption versus uncertainty introduced by the dissipation closure in conventional two-equation LEV models.

### ACKNOWLEDGMENTS

This work was funded by the Strategic Basic Research project titled Efficient Uncertainty Quantification for Optimization and Robust Design in Industrial Applications (EUFORIA, Grant No. IWT-140068).

### APPENDIX: THE REYNOLDS STRESS SHAPE PERTURBATION (RSSP) METHOD

The RSSP method was first proposed by Emory *et al.* [13] to quantify uncertainty in QoIs related to mean momentum transport by turbulence. This Appendix briefly summarizes the method.

A Reynolds stress tensor  $R_{ij} \equiv \overline{u_i' u_j'}$  can be eigendecomposed as

$$R_{ij} = 2k(\delta_{ij}/3 + V_{ik} V_{jl} \Lambda_{kl}), \quad (\text{A1})$$

with  $[\Lambda_{ij}] = \text{diag}[\lambda_1, \lambda_2, \lambda_3]$  ( $\lambda_1 + \lambda_2 + \lambda_3 = 0$  and  $\lambda_1 \geq \lambda_2 \geq \lambda_3$ ), representing the shape of  $R_{ij}$ , and  $V_{ij}$  an orthogonal tensor representing the orientation of  $R_{ij}$ . Under the realizability constraint, there are three limiting states: the one-component limit with  $[\Lambda_{ij}^{\text{C1}}] = \text{diag}[2/3, -1/3, -1/3]$ , the two-component limit with  $[\Lambda_{ij}^{\text{C2}}] = \text{diag}[1/6, 1/6, -1/3]$ , and the three-component (i.e., isotropic) limit with  $[\Lambda_{ij}^{\text{C3}}] = \text{diag}[0, 0, 0]$ . The shape  $\Lambda_{ij}$  of any realizable  $R_{ij}$  can thereby be uniquely expressed by a convex combination of  $\Lambda_{ij}^{\text{C1}}$ ,  $\Lambda_{ij}^{\text{C2}}$ , and  $\Lambda_{ij}^{\text{C3}}$  as

$$\Lambda_{ij} = s_1 \Lambda_{ij}^{\text{C1}} + s_2 \Lambda_{ij}^{\text{C2}} + s_3 \Lambda_{ij}^{\text{C3}}, \quad s_1, s_2, s_3 \geq 0, \quad s_1 + s_2 + s_3 = 1. \quad (\text{A2})$$

Equation (A2) can be graphically represented by a barycentric map, in Fig. 18, where the three corners represent the limit shapes and any realizable  $\Lambda_{ij}$  should be inside the triangle.

The RSSP method proposes to perturb the Reynolds stress by changing its shape and orientation within the realizable constraints. The perturbed Reynolds stress, denoted by  $\tilde{R}_{ij}$ , is thus expressed as

$$\tilde{R}_{ij} = 2k(\delta_{ij}/3 + \tilde{V}_{ik} \tilde{V}_{jl} \tilde{\Lambda}_{kl}). \quad (\text{A3})$$

To estimate the bounds of a QoI, it has been proposed that one can simply preserve the orientation  $V_{ij}$  of the Reynolds stress  $R_{ij}$  resulting from a baseline LEV model while perturbing the shape  $\Lambda_{ij}$  linearly towards  $\Lambda_{ij}^{\text{C1}}$ ,  $\Lambda_{ij}^{\text{C2}}$ , and  $\Lambda_{ij}^{\text{C3}}$ , respectively, as illustrated in Fig. 18 [12,13,15]. The perturbed eigenvalues and eigenvectors are then given by

$$\tilde{\Lambda}_{ij} = (1 - m) \Lambda_{ij} + m \Lambda_{ij}^{\text{C1/C2/C3}}, \quad \tilde{V}_{ij} = V_{ij}, \quad (\text{A4})$$

where  $m \in [0, 1]$  is a free parameter controlling the perturbation magnitude. Among all the routes of perturbing  $\Lambda_{ij}$  under the realizability constraint, the perturbation linearly towards  $\Lambda_{ij}^{\text{C1}}$  (or  $\Lambda_{ij}^{\text{C3}}$ )

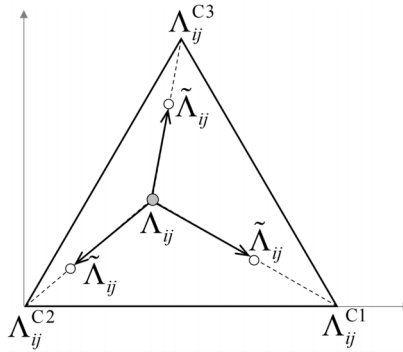


FIG. 18. Principle of the Reynolds-stress-shape-perturbation (RSSP) method represented in the barycentric map.

as Eq. ((A4) b) is the most effective route to increase (or decrease) the shear stress magnitude in a parallel shear turbulence as well as the energy production rate  $\mathcal{P}$  [12,13,15]. These two factors directly influence the general level of mean momentum transport. Therefore, it is reasonable to expect that the results of the perturbations towards  $\Lambda_{ij}^{C1}$  and  $\Lambda_{ij}^{C3}$  will provide bounds for a QoI related to momentum transport.

For correcting the underestimated energy behind bluff bodies in this paper, we select the perturbation towards  $\Lambda_{ij}^{C1}$  (the most effective route to increase the energy production) and compare its performance with the DSDL model. The parameter  $m$  is set to be 0.5, which is approximately the largest value that yields a converged steady solution.

- 
- [1] S. H. Cheung, T. A. Oliver, E. E. Prudencio, S. Prudhomme, and R. D. Moser, Bayesian uncertainty analysis with applications to turbulence modeling, *Reliab. Eng. Syst. Safety* **96**, 1137 (2011).
  - [2] T. A. Oliver and R. D. Moser, Bayesian uncertainty quantification applied to RANS turbulence models, *J. Phys.: Conf. Ser.* **318**, 042032 (2011).
  - [3] W. Edeling, P. Cinnella, R. P. Dwight, and H. Bijl, Bayesian estimates of parameter variability in the  $k-\epsilon$  turbulence model, *J. Comput. Phys.* **258**, 73 (2014).
  - [4] W. Edeling, P. Cinnella, and R. P. Dwight, Predictive RANS simulations via Bayesian model-scenario averaging, *J. Comput. Phys.* **275**, 65 (2014).
  - [5] M. Shirzadi, P. A. Mirzaei, and M. Naghashzadegan, Improvement of  $k$ -epsilon turbulence model for CFD simulation of atmospheric boundary layer around a high-rise building using stochastic optimization and Monte Carlo sampling technique, *J. Wind Eng. Ind. Aerodynamics* **171**, 366 (2017).
  - [6] T. Oliver and R. Moser, Uncertainty quantification for RANS turbulence model predictions, APS Division of Fluid Dynamics Meeting Abstracts **62**, LC-004 (2009).
  - [7] E. Dow and Q. Wang, Quantification of structural uncertainties in the  $k-w$  turbulence model, in *52nd AIAA/ASME/ASCE/AHS/ASC Structures, Structural Dynamics and Materials Conference, 19th AIAA/ASME/AHS Adaptive Structures Conference* (AIAA, Reston, VA, 2011), 13t, p. 1762.
  - [8] B. D. Tracey, K. Duraisamy, and J. J. Alonso, A machine learning strategy to assist turbulence model development, in *53rd AIAA Aerospace Sciences Meeting* (AIAA, Reston, VA, 2015), p. 1287.
  - [9] K. Duraisamy, Z. J. Zhang, and A. P. Singh, New approaches in turbulence and transition modeling using data-driven techniques, in *53rd AIAA Aerospace Sciences Meeting* (AIAA, Reston, VA, 2015), p. 1284.
  - [10] A. P. Singh and K. Duraisamy, Using field inversion to quantify functional errors in turbulence closures, *Phys. Fluids* **28**, 045110 (2016).

- [11] M. Emory, R. Pecnik, and G. Iaccarino, Modeling structural uncertainties in Reynolds-averaged computations of shock/boundary layer interactions, in *49th AIAA Aerospace Sciences Meeting including the New Horizons Forum and Aerospace Exposition* (AIAA, Reston, VA, 2011), p. 479.
- [12] C. Górlé, C. M. Emory, J. Larsson, and G. Iaccarino, Epistemic uncertainty quantification for RANS modeling of the flow over a wavy wall, *Annual Research Briefs* (Center for Turbulence Research, 2012), pp. 81–91.
- [13] M. Emory, J. Larsson, and G. Iaccarino, Modeling of structural uncertainties in Reynolds-averaged Navier-Stokes closures, *Phys. Fluids* **25**, 110822 (2013).
- [14] G. Iaccarino, A. A. Mishra, and S. Ghili, Eigenspace perturbations for uncertainty estimation of single-point turbulence closures, *Phys. Rev. Fluids* **2**, 024605 (2017).
- [15] C. Górlé, S. Zéoli, M. Emory, J. Larsson, and G. Iaccarino, Epistemic uncertainty quantification for Reynolds-averaged Navier-Stokes modeling of separated flows over streamlined surfaces, *Phys. Fluids* **31**, 035101 (2019).
- [16] H. Xiao, J.-L. Wu, J.-X. Wang, R. Sun, and C. Roy, Quantifying and reducing model-form uncertainties in Reynolds-averaged Navier-Stokes simulations: A data-driven, physics-informed bayesian approach, *J. Comput. Phys.* **324**, 115 (2016).
- [17] J. Wang, J.-L. Wu, and H. Xiao, Incorporating prior knowledge for quantifying and reducing model-form uncertainty in RANS simulations, *Intl. J. Uncert. Quantif.* **6**, 109 (2016).
- [18] W. Edeling, G. Iaccarino, and P. Cinnella, A return to eddy viscosity model for epistemic UQ in RANS closures, [arXiv:1705.05354](https://arxiv.org/abs/1705.05354).
- [19] W. N. Edeling, G. Iaccarino, and P. Cinnella, Data-free and data-driven RANS predictions with quantified uncertainty, *Flow Turb. Combust.* **100**, 593 (2018).
- [20] H. Xiao, J.-X. Wang, and R. G. Ghanem, A random matrix approach for quantifying model-form uncertainties in turbulence modeling, *Comput. Methods Appl. Mech. Eng.* **313**, 941 (2017).
- [21] S. Zeoli, Numerical simulation of turbulent flows with application to wind engineering problems, Ph.D. thesis, Faculté Polytechnique, Université de Mons, 2018.
- [22] Z. Hao and C. Górlé, Quantifying turbulence model uncertainty in Reynolds-averaged Navier-Stokes simulations of a pin-fin array. Part 1: Flow field, *Comput. Fluids* **209**, 104641 (2020).
- [23] A. Parente, C. Górlé, J. Van Beeck, and C. Benocci, Improved  $k-\varepsilon$  model and wall function formulation for the RANS simulation of ABL flows, *J. Wind Eng. Indust. Aerodynam.* **99**, 267 (2011).
- [24] E. Garnier, P. Pamart, J. Dandois, and P. Sagaut, Evaluation of the unsteady RANS capabilities for separated flows control, *Comput. Fluids* **61**, 39 (2012).
- [25] J. Eaton and J. Johnston, Turbulent flow reattachment: An experimental study of the flow and structure behind a backward-facing step, Stanford Univ. Rep., MD-39, 1980.
- [26] A. S. Neto, D. Grand, O. Métais, and M. Lesieur, A numerical investigation of the coherent vortices in turbulence behind a backward-facing step, *J. Fluid Mech.* **256**, 1 (1993).
- [27] R. L. Simpson, Aspects of turbulent boundary-layer separation, *Prog. Aerosp. Sci.* **32**, 457 (1996).
- [28] H. Le, P. Moin, and J. Kim, Direct numerical simulation of turbulent flow over a backward-facing step, *J. Fluid Mech.* **330**, 349 (1997).
- [29] J.-P. Bonnet and J. Delville, Review of coherent structures in turbulent free shear flows and their possible influence on computational methods, *Flow, Turbul. Combust.* **66**, 333 (2001).
- [30] H. Ha Minh, Semi-deterministic turbulence modelling for flows dominated by strong organised structures, in *Proceedings of the 9th International Symposium on Turbulent Shear Flows, Kyoto, Japan, 1994*, Vol. 1 (Springer, New York, 1994), pp. 5–10.
- [31] A. Travin, M. Shur, M. Strelets, and P. Spalart, On URANS solutions with LES-like behaviour, in *ECCOMAS 2004-European Congress on Computational Methods in Applied Sciences and Engineering* (2004).
- [32] B. A. Younis and Y. Zhou, Accounting for mean-flow periodicity in turbulence closures, *Phys. Fluids* **18**, 018102 (2006).
- [33] S. S. Girimaji, Partially-averaged Navier-Stokes model for turbulence: A Reynolds-averaged Navier-Stokes to direct numerical simulation bridging method, *J. Appl. Mech.* **73**, 413 (2006).

- [34] F. Menter and Y. Egorov, The scale-adaptive simulation method for unsteady turbulent flow predictions. Part 1: Theory and model description, *Flow, Turbul. Combust.* **85**, 113 (2010).
- [35] I. Castro and A. Haque, The structure of a turbulent shear layer bounding a separation region, *J. Fluid Mech.* **179**, 439 (1987).
- [36] R. D. Moser and M. Rogers, Mixing transition and the cascade to small scales in a plane mixing layer, *Phys. Fluids A: Fluid Dyn.* **3**, 1128 (1991).
- [37] M. M. Rogers and R. D. Moser, The three-dimensional evolution of a plane mixing layer: The Kelvin-Helmholtz rollup, *J. Fluid Mech.* **243**, 183 (1992).
- [38] M. M. Rogers and R. D. Moser, Spanwise scale selection in plane mixing layers, *J. Fluid Mech.* **247**, 321 (1993).
- [39] R. D. Moser and M. M. Rogers, The three-dimensional evolution of a plane mixing layer: Pairing and transition to turbulence, *J. Fluid Mech.* **247**, 275 (1993).
- [40] A. Townsend, *Turbulent Shear Flow* (Cambridge University Press, Cambridge, 1980).
- [41] A. K. M. F. Hussain and W. C. Reynolds, The mechanics of an organized wave in turbulent shear flow, *J. Fluid Mech.* **41**, 241 (1970).
- [42] K. Hanjalic, B. E. Launder, and R. Schiestel, Multiple-time-scale concepts in turbulent transport modeling, in *Symposium on Turbulent Shear Flows, 2nd, London, England, 2-4 July 1979* (Imperial College of Science and Technology, London, 1979), pp. 10.31–10.36.
- [43] W. Jones and B. E. Launder, The prediction of laminarization with a two-equation model of turbulence, *Intl. J. Heat Mass Transf.* **15**, 301 (1972).
- [44] D. C. Wilcox, *Turbulence Modeling for CFD*, Vol. 2 (DCW Industries, La Canada, CA, 1998), Chap. 3.
- [45] B.S. Baldwin and H. Lomax, Thin layer approximation and algebraic model for separated turbulent flows, in *16th AIAA Aerospace Sciences Meeting, Huntsville, Alabama* (AIAA, Reston, VA, 1978), paper AIAA 78-257.
- [46] S.-W. Kim and C.-P. Chen, A multiple-time-scale turbulence model based on variable partitioning of the turbulent kinetic energy spectrum, *Numer. Heat Transfer, Part B* **16**, 193 (1990).
- [47] R. Schiestel, *Modeling and Simulation of Turbulent Flows*, Vol. 4 (John Wiley & Sons, New York, 2010), Sec. 18.3.
- [48] A. Favre, L. Kovaszny, R. Dumas, J. Gaviglio, and M. Coantic, *Turbulence in Fluid Mechanics: Theoretical and Experimental Foundations; Statistical Methods* (Gauthier-Villars, Paris, 1976), p. 429.
- [49] R. Schiestel, Multiple-time-scale modeling of turbulent flows in one-point closures, *Phys. Fluids* **30**, 722 (1987).
- [50] J. Rotta, Statistical theory of non-homogeneous turbulence, *J. Phys.* **129**, 547 (1951).
- [51] M. Kato, The modelling of turbulent flow around stationary and vibrating square cylinders, *Turb. Shear Flow* **1**, 10 (1993).
- [52] W. C. Strahle, Stagnation point flows with free stream turbulence-the matching condition, *AIAA J.* **23**, 1822 (1985).
- [53] B. E. Launder and B. Sharma, Application of the energy-dissipation model of turbulence to the calculation of flow near a spinning disc, *Lett. Heat Mass Transf.* **1**, 131 (1974).
- [54] F. R. Menter, Review of the shear-stress transport turbulence model experience from an industrial perspective, *Intl. J. Comput. Fluid Dyn.* **23**, 305 (2009).
- [55] H. G. Weller, G. Tabor, H. Jasak, and C. Fureby, A tensorial approach to computational continuum mechanics using object-oriented techniques, *Comput. Phys.* **12**, 620 (1998).
- [56] L. Lourenco and C. Shih, Characteristics of the plane wake of a circular cylinder: A particle image velocity study (1993). Reported by A.G. Kravchenko and P. Moin in “Numerical studies of flow over a circular cylinder at  $Re_D=3900$ ”, *Phys. Fluids* **12**, 403 (2000).
- [57] M. Breuer, Large eddy simulation of the subcritical flow past a circular cylinder: Numerical and modeling aspects, *Intl. J. Numer. Methods Fluids* **28**, 1281 (1998).
- [58] D. Durao, M. Heitor, and J. Pereira, Measurements of turbulent and periodic flows around a square cross-section cylinder, *Expt. Fluids* **6**, 298 (1988).
- [59] F. E. Ames, L. A. Dvorak, and M. J. Morrow, Turbulent augmentation of internal convection over pins in staggered-pin fin arrays, *J. Turbomachinery* **127**, 183 (2005).

- [60] Z. Hao and C. Gorié, Large eddy simulations of forced heat convection in a pin-fin array with *a priori* examination of an eddy-viscosity turbulence model, [Intl. J. Heat Fluid Flow](#) **77**, 73 (2019).
- [61] M. J. Lee and W. C. Reynolds, Numerical Experiments on the Structure of Homogeneous Turbulence (Thermosciences Div., Dept. of Mech. Eng., Stanford University, Stanford, CA, 1985).
- [62] J. D. Schwarzkopf, D. Livescu, J. R. Baltzer, R. A. Gore, and J. Ristorcelli, A two-length scale turbulence model for single-phase multi-fluid mixing, [Flow Turb. Combust.](#) **96**, 1 (2016).
- [63] H. Xiao and P. Cinnella, Quantification of model uncertainty in RANS simulations: A review, [Prog. Aerosp. Sci.](#) **108**, 1 (2019).